Advanced Composites and Hybrid Materials (2018) 1:748–758
https://doi.org/10.1007/s42114-018-0055-0

ORIGINAL RESEARCH

Optical and photoelectrochemical studies on photoactive inorganic/organic/organic/interface assemblies of CdS/poly 3-(2-thienyl) aniline/poly 2,2 bithiophene

Kasem K. Kasem [1] · Henry Worley [1] · Mary Elmasry [1]

Received: 20 December 2017 / Accepted: 8 August 2018 / Published online: 10 September 2018

Abstract
Assemblies of poly 2,2 bithiophene, poly 3-(2-thienyl) aniline, and CdS were subjected to optical and photoelectrochemical investigation in acetate, citrate, and phosphate aqueous electrolytes. Optical conductivity and dielectric contents reflect the role of CdS on the optical properties of the assemblies. Occlusion of CdS into the organic polymer increased the electron diffusion coefficient and diffusion length by changing both the electron lifetime and electron transport time. O_2 enhanced generated photocurrent in presence and in absence of a magnetic field. The magnetic field effects were explained on the basis that external magnetic fields affect the photogeneration of singlet/triplet radical pair processes. The recorded photoactivities indicate formation of hybrid sub-bands due to band alignments between each of the assembly components. The present study also shows that the use of electrolytes can affect the electron life-times at I/O/O/I and possible charge transfer processes.

Keywords Cadmium sulfide · Photoelectrochemistry · Photoactive interfaces · Organic semiconductors · Magnetic effects

1 Introduction

Creation of hybrid interfaces such as at the heterojunctions of inorganic/organic (IOI) or organic/organic interfaces (OOI) has attracted attention because of its potential applications in spintronics, drug delivery using nanoparticles, and solar energy harvesting [1–9]. The heterojunctions in these assemblies can affect their chemical, electrochemical, optical, magnetic, and mechanical properties. Surface modification through the formation of these interfaces can also be a very effective way to create or eliminate defects and alter the energy bands at inorganic/organic interfaces. Surface modification will also alter the donor/acceptor character of these assemblies. The charge production, separation, and transfer at these interfaces was the subject of several investigations [10–18]. Some investigations were focused on the study of the magnitude of the barrier for charge (hole or electron) injection and the band energy alignments at these interfaces [10–14].

Energy-level alignment at different photoactive interfaces, such as in organic/organic assemblies [11, 14], has been investigated. Assemblies involving cadmium chalcogenides such as CdSe, CdS with polythiophenes, and other photoactive organic compounds [15–18]. Further, carbon nanotubes in interface with CoS_2 [19] and N-based organic polymers interfaced with ZnS [20] or organic/metal assemblies [21] were investigated. Using these interfaces to build organic electronics or hybrid organic solar cells [10, 18, 22] has been achieved.

Building photoactive assemblies of hybrid thin film interfaces can be done by methods such as the layer-by-layer method, co-electrodeposition, and occlusion electrodeposition (OE). However, when the guest material is inactive to oxidative or reductive electrodeposition, and when co-electrodeposition would involve multiple steps that might alter the final composition of the hybrid films, OE is the optimum solution. Composite films containing occluded TiO_2 [23–25] or CdS [26, 27] particles within a Ni matrix have been previously prepared using an occlusion method. Other metal matrices such as Ni, Cu, Ag, and In [28] and organic matrices such as poly-pyrrole [29] have also been used for immobilizing TiO_2 particles.

✉ Kasem K. Kasem
kkasem@iuk.edu

[1] School of Sciences, Indiana University Kokomo, Kokomo, IN 46904, USA

Polythiophene, polyaniline, and their derivatives have noticeable stability, good electrical conductivity, and excellent electrochromic properties. These properties makes them useful components in electronic devices and electrode materials in solar harvesting cells.

The monomers 2,2 bithiophene (BTh) and 3-(2-thienyl) aniline (ThA) as derivatives of thiophene and aniline were used to prepare their corresponding polymers: poly 2,2 bithiophene (PBTh) and poly 3-(2-thienyl) aniline (PThA), respectively. The combination of ionic sulfur in CdS with covalent sulfur in organic polymers may affect the charge transfer processes in assemblies containing these systems. In this paper, we aimed to investigate what differences in optical and photoelectrochemical behaviors can be caused by the occlusion of CdS in organic polymers PThA and PBTh. In particular, we studied the changes in the photocurrent generation as an indicator for this assembly's ability to cause the photoinduced charge separation. The host matrix was produced by electropolymerization of 2,2 bithiophene (BTh) which forms polymeric networks suitable for efficient occlusion. The optical parameters such as the optical conductivity (σ_{opt}), optical absorption coefficient (α), refractive index (n), extinction coefficients (k), real dielectric constants (ε_r), and imaginary dielectric constants (ε_i) were also investigated. Furthermore, we explored the possible effects that can be caused by applying a magnetic field to the assembly.

2 Experimental

2.1 Reagents

All the reagents were of analytical grade. All of the solutions were prepared using deionized (DI) water unless otherwise stated.

2.2 Preparations

The O/O/II thin films were prepared as follows:

1. Photopolymerization of 3-(2-thienyl) aniline (ThA) on CdS nanoparticles to create an I/O/I of CdS/PThA

Colloidal suspensions of CdS coated with/PThA (CdS/PThA) interface were prepared as follows: 0.05 g of CdS nanoparticles prepared as reported previously [30] were suspended in the solution of ThA in acetonitrile. The mixture was subjected to a 10-min sonication followed by stirring for 1.0 h to allow maximum adsorption of ThA on the CdS nanoparticles. The excess PThA was removed by centrifugation. CdS nanoparticles with adsorbed PThA were re-suspended in deionized (DI) water containing few drops of H_2O_2 and subjected to UV radiation under constant stirring for 3.0 h. The resultant CdS/PThA was rinsed several times with DI water and allowed to dry at 120 °C for 2.0 h. The product of this step was used for the occlusion electrodeposition process.

2. Occlusion method

Thin films of CdS/PThA/PBTh were generated electrochemically using cyclic voltammetry (CV) by repetitive cycling of the FTO electrode's potential between − 0.5 and 1.7 V vs Ag/AgCl in an acetonitrile suspension of PThA/CdS and 1 mM of the BTh monomer and 0.5 M $LiClO_4$.

2.3 Instrumentation

All electrochemical experiments were carried out using a conventional three-electrode cell consisting of a Pt wire as a counter electrode, Ag/AgCl as a reference electrode, and FTO with surface area 2.0 cm^2 as working electrode. Photoelectrochemical studies on the thin solid films were performed on an experimental setup as illustrated in Fig. 1. A BAS 100-W electrochemical analyzer (Bioanalytical Co.) was used to perform the electrochemical studies. Optical parameters were carried out studying the steady-state reflectance spectra using a Shimadzu UV-2101PC spectrophotometer. An Olympus BX-FL reflected light fluorescence microscope working with polymerized light at wavelengths ranging between 330 and 550 nm was used to explore surface imaging of the film. Irradiation was performed with a solar simulator 300.0-W xenon lamp (Newport, NJ) with an IR filter. Magnetic measurements were performed using a Frederiksen digital Tesla meter − 4060.50, with 0.01–2 T, with 1-mT resolution.

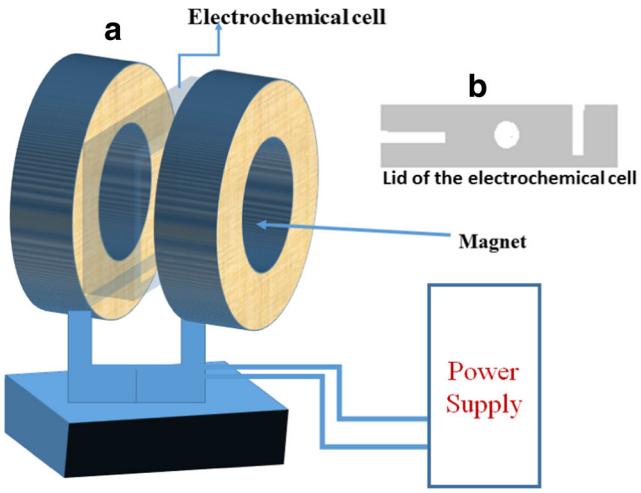

Fig. 1 **a** Magnetic field source applied on the electrochemical cell. **b** The lid for the electrochemical cell that gives the option of making the magnetic field parallel or perpendicular to the electrode surface

2.4 Photolysis cell

The electrolysis cell was a one-compartment Pyrex cell with a quartz window facing the irradiation source.

2.5 Measurement of electron lifetime (τ_n) in an organic/organic/inorganic interface

Because electron lifetime plays an important role in energy conversion efficiency in solar cells, we used the following equation that relate τ_n with the open circuit potential (V_{oc}) decay [31]:

$$\tau_n = -(k_B\, T/e) \times (dV_{oc}/dt)^{-1} \quad (1)$$

where k_B is the Boltzmann constant, e is the electron charge, T is the temperature in K, and V_{oc} is the open circuit potential in volts.

2.6 Magnetic field effects

Magnetic excitation was created by placing the FTO (2 mm thick), modified with the CdS/PThA/PBTh in parallel to the magnetic field generated by two circular disk magnets with a power of 0.200 T. The cell was positioned to face the light source as shown in Fig. 1. The magnetic field was measured by placing the Tesla meter on the assembly's surface before immersing it into the electrolyte. For comparison, the current and potential generated in the absence of the magnetic field were also measured.

3 Results and discussion

3.1 Optical studies

Optical parameters such as σ_{opt}, α, n, k, ε_r, and ε_i have been calculated and plotted as a function of photon energy. The results are displayed in Figs. 2, 3, 4, 5, and 6.

3.1.1 Optical band gap studies

The results displayed in Fig. 2a are the absorption spectra of the CdS/PThA/PBTh assembly, and of the host polymer PBTh where absorption is plotted against photon energy of incident light. Figure 2b, c were prepared after treatment of the absorption data as plots of $\alpha^{1/2}$ vs photon energy (hν) and $(\alpha \times h\nu)^2$ vs hν respectively as described in previous studies [32]. The value of α was calculated using a film thickness of 1.0 μm. Both the host polymer, PBTh, and the assembly show greater absorption in the range of photon energies between 2.3 and 2.6 eV. The results also indicate that the range of absorbance of the assembly is greater than that of the host polymer PBTh. This can be attributed to the closer band gap of CdS and of PThA.

Further analysis of Fig. 2a has been performed using Tauc plots. Figure 2b shows that the indirect band gap in PBTh is larger than that of the assembly. This is because the occlusion of CdS modified with PThA created hybrid sub-bands with smaller band gaps between the highest occupied molecular orbitals (HOMO) and lowest unoccupied molecular orbitals (LUMO) of the host polymer. Furthermore, the plot of photon energy vs $(\alpha \times h\nu)^2$ (Fig. 2c) confirms the same phenomena discussed in Fig. 2b. The direct band gap of PBTh is greater than that of the CdS/PThA/PBTh assembly.

3.1.2 Optical parameters

a) Refractive index, n, extinction coefficient, k

Figure 3a displays the plot of extinction coefficient k vs photon energy. Figure 3a indicates (1) the value of k of PBTh is greater than that of CdS/PThA/PBTh, (2) the value of k increased when the photon energy for both materials was increased, and (3) the value of k shows a sharp increase at a photon energy greater than 2 eV. Figure 3b displays the plot of refractive index n vs photon energy. Although both materials

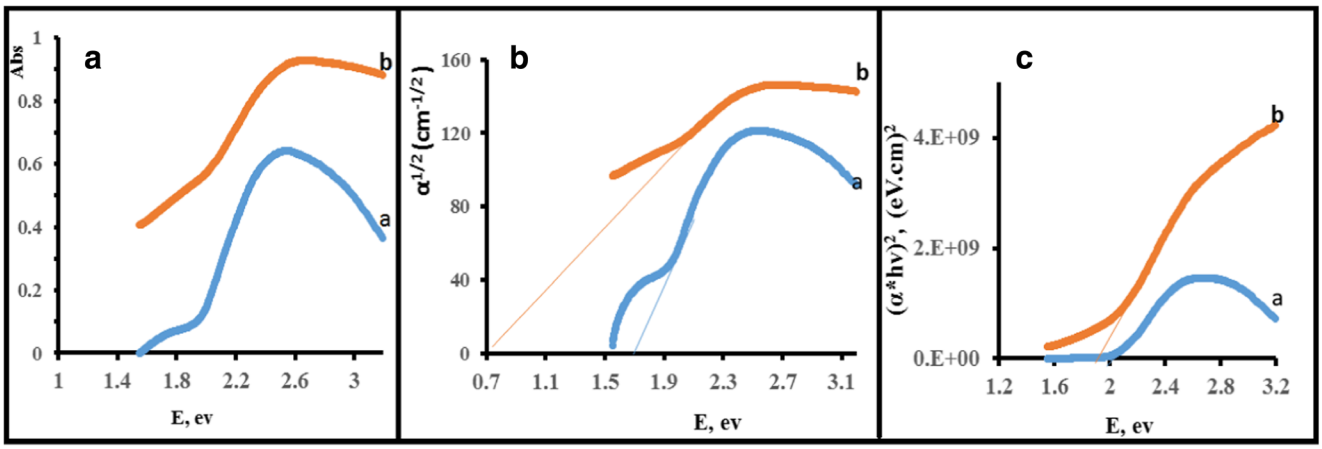

Fig. 2 **a** Absorption spectra of (a) PBTh and (b) CdS/PThA/PBTh. **b** $\alpha^{1/2}$ ($cm^{-1/2}$) vs photon energy. **c** $(\alpha \times h\nu)^2$, (eV cm)^2 vs photon energy

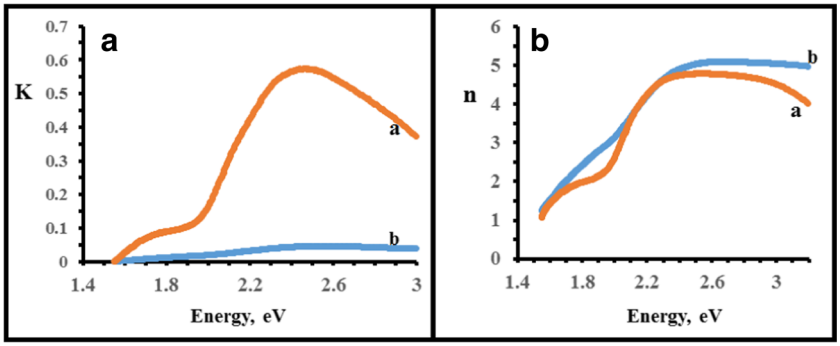

Fig. 3 **a** Extinction coefficient k vs photon energy. **b** Refractive index n vs photon energy of (a) PBTh and (b) CdS/PThA/PBTh

exhibit a large increase in n when the photon's energy is greater than 2.0 eV, the value of n for CdS/PThA/PBTh is slightly greater than that of PBTh.

b) Dielectric constants, real ε_r and imaginary ε_i

The calculated ε_r and ε_i are plotted against photon energy. The results are displayed in Fig. 4a, b. Figure 4a shows that the change in ε_i vs photon energy follows the same pattern described in Fig. 3a, due to the direct relation with k ($\varepsilon_i = 2nk$). The plot of the ε_r vs photon energy is displayed in Fig. 4b. This figure shows a pattern similar to that displayed n in Fig. 3b. As ε_r was calculated from the relation $\varepsilon_r = n^2 - k^2$, and as $n \gg k$, we can approximate that ε_r is directly proportional to n.

The results displayed in these figures show that the ε_i of CdS/PThA/PBTh assembly is less than that calculated for PBTh (host polymer). Because ε_i is associated with dissipation of energy into the medium, the modified CdS nanoparticles occluded into PBTh inhibit the energy dissipation process [33]. The ε_i is indication of the influence of dipole motion on energy absorption by the dielectric material from an electric field. Figure 4b shows that the ε_r of PBTh and that of CdS/PThA/PBTh assembly have closer values around a photon energy range between 1.9 and 2.3 eV. Above and below this range, the real dielectric part for CdS/PThA/PBTh exceeds that of PBTh. As the real part of the dielectric is related to polarization and anomalous dispersion, it indicates how much occlusion of CdS/PThA slows down the speed of light in the material [34].

The ratio $\varepsilon_i/\varepsilon_r$ is called loss factor and was calculated for both PBTh and CdS/PThA/PBTh assemblies. Figure 5 displays the loss factor vs photon energy. The occlusion of CdS/PThA into the matrix of PBTh contributes to the decrease of ε_i, and the increase of ε_r.

c) Optical conductivity σ_{opt}

Calculated σ_{opt} as described in previous work [34] are displayed in Fig. 6. The decrease of σ_{opt} with increasing photon energy is due to the presence of modified CdS nanoparticles as a dopant in PBTh network structure. Figure 6b indicates that the dopant lacks the ability to provide the host polymer with an additional charge transfer [35]. The interaction between incident light and charges of the material will take place as a result of absorption of photon energy by the assembly [36]. Modified CdS impeded the process that leads to polarizing the charges of the material. This means that the CdS/PThA/PBTh negatively affected the dissipation of energy into the host PBTh film. This is consistent with the results for imaginary part vs photon energy displayed in Fig. 4a.

3.2 Photoelectrochemical behavior

Photoelectrochemistry of the host polymer PBTh has been discussed in previous work [37]. For comparison, we used this

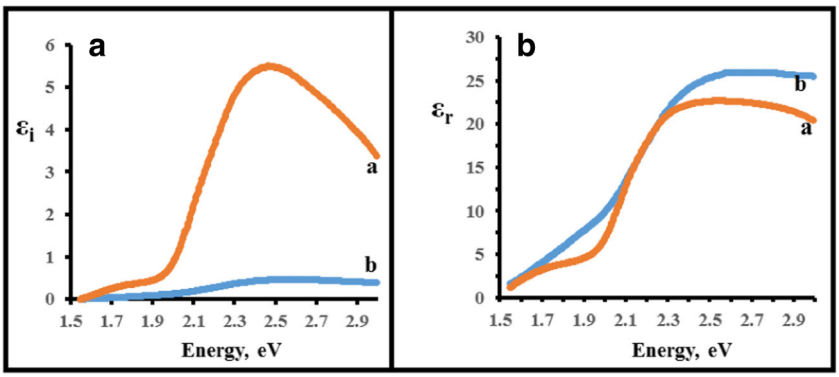

Fig. 4 **a** Imaginary ε_i and **b** real ε_r components of dielectric constant. (a) PBTh and (b) CdS/PThA/PBTh

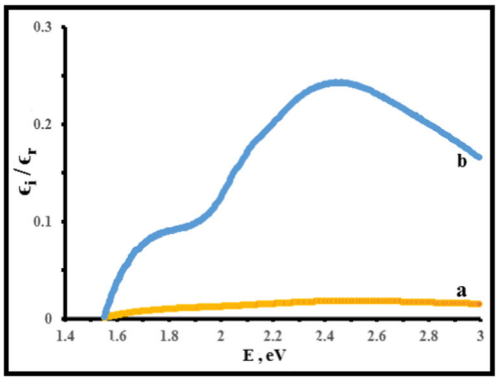

Fig. 5 Loss factor ($\varepsilon_i/\varepsilon_r$) vs photon energy for (a) PBTh and (b) CdS/PThA/PBTh

information to conclude the contribution of the occluded CdS/PThA nanoparticles to the photoactivity outcome of the whole assembly. Unless otherwise stated, the photoelectrochemical behavior was investigated in the dark and under illumination by cycling the potential of FTO/CdO_2/CdO/PBTh between − 1.0 and 1.0 V vs Ag/AgCl at a scan rate of 0.10 V/s in a given electrolyte.

3.2.1 Electrochemical behavior of the FTO/CdS/PThA/PBTh assembly in aqueous acetate electrolyte

The behavior of the FTO/CdS/PThA/PBTh assemblies was investigated in 0.2 M acetate electrolyte (pH 8). Figure 7a shows that in the cathodic scan at ≈ 0.20 vs Ag/AgCl, the recorded photocurrent is greater than the current recorded in the dark. These results indicate that the approximate E_{fb} (flat band potential) of the assembly is at 0.20 V or 0.40 V vs SHE. (Table 1). However, in the anodic scan, the photocurrent recorded is smaller than that in cathodic scan and exceeds the current recorded in the dark at ≈0.20 vs Ag/AgCl. We assume that 0.40 V vs SHE is the value of the hybrid sub-band created upon occlusion of CdS nanoparticles in PThA suspended within an acetate electrolyte. Figure 7b shows the photocurrent-time curve generated by subjecting the FTO/CdS/PThA/PBTh assembly to a constant potential (− 0.5 V vs Ag/AgCl) under

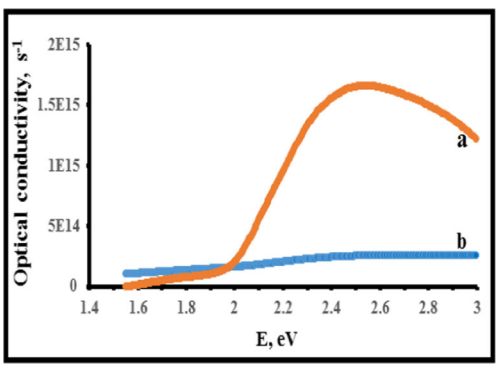

Fig. 6 Optical conductivity vs photon energy for (a) PBTh and (b) CdS/PThA/PBTh

illumination for a long duration. Upon illumination of an oxygenated electrolyte, a sudden increase in the current (≈ 16 μA) followed by a slight increase in the photocurrent is indicated by the formation of a positive linear slope (Fig. 7b (a)). When the electrolyte was deoxygenated (using N_2 gas), the illumination generated less photocurrent and a more negative linear slope than that observed with the presence of O_2 (Fig. 7b (b)). Such behavior was reproducible. It is important to notice that the absence of O_2 decreased the photocurrent and reduced the capacitive current as evident from the smaller dark current in deoxygenated electrolyte than in the oxygenated electrolyte. When a magnetic field was applied, the photocurrent vs time outcome is shown in Fig. 7b-inset box. It should be noticed that (1) these photocurrent curves generated in the presence and in the absence of O_2 indicate the importance of O_2 role in enhancing charge separation during the illumination period (in absence of O_2, photocurrent decreases), (2) the magnetic field's only effect is elimination of the low frequency noises, shown in the recorded photocurrent in the absence of O_2., (3) the magnitude of the photocurrent did not change upon applying the magnetic field, and (4) a small increase in the capacitive current was observed.

3.2.2 Electrochemical behavior of the FTO/CdS/PThA/PBTh assembly in aqueous citrate electrolytes

The electrochemical behavior of FTO/CdS/PThA/PBTh was investigated in aqueous citrate electrolyte (pH 8) in the dark and under illumination. The results are displayed in Fig. 8. This shows that at 0.25 V vs Ag/AgCl, the photocurrent exceeds the current recorded in the dark for citrate electrolyte (Fig. 8a) in the cathodic scan, and at ≈ 0.35 V in the anodic scan. We assume that 0.45 V vs SHE is the value of the hybrid sub-band created upon occlusion of CdS nanoparticles in PThA in the citrate electrolyte.

The photocurrent vs time curve generated by subjecting the FTO/CdS/PThA/PBTh assembly to long-time illumination under a constant potential (− 0.500 V vs Ag/AgCl). A behavior comparable to that observed in Fig. 7b (acetate electrolyte) was recorded in Fig. 8b. However, upon illumination of the oxygenated citrate electrolyte (Fig. 8b), a sharp anodic current spike is observed. Such behavior can be explained by fast charge recombination because of hole accumulations at the outermost layers of the assembly/electrolyte interface [38]. Such phenomena were more noticeable in the deoxygenated electrolyte (Fig. 8b (b)). When the light is off, there is no evidence for reversed transient current. This means that no backflow of electrons from the substrate FTO to the assembly body took place.

When the electrolyte was deoxygenated, illumination generated much less photocurrent (10–12 μA). Such behavior was reproducible through multiple cycles of illumination and darkness. When a magnetic field was applied (Fig. 8b-inset box), the recorded photocurrent in the deoxygenated

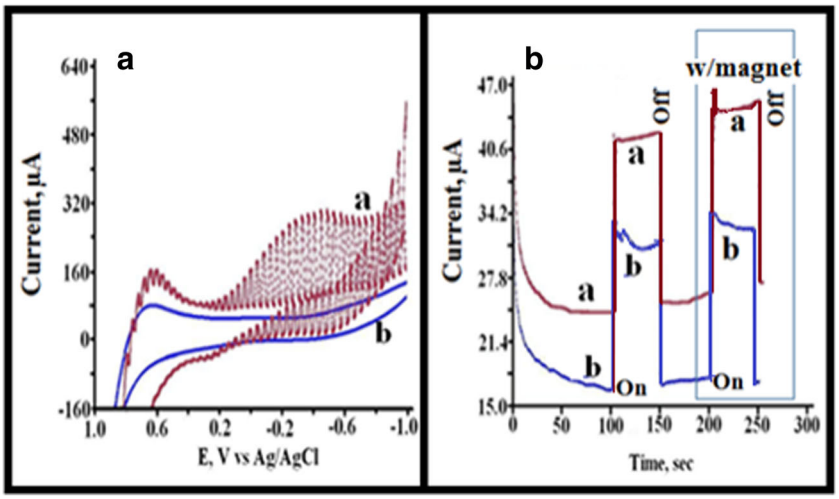

Fig. 7 Photoelectrochemical behavior of FTO/CdS/PThA/PBTh in 0.2 M acetate electrolyte **a** CV at 0.1 V/s, (a) illumination, (b) dark. **b** Photocurrent vs time curve at − 0.5 V vs Ag/AgCl (a) with O_2 and (b) after purge with N_2 in frame curves were collected in the presence of a magnetic field

citrate electrolyte was less than that in the absence of magnetic field). The assembly generated more photocurrent in citrate than in acetate electrolyte.

3.2.3 Electrochemical behavior of the FTO/CdS/PThA/PBTh assembly in aqueous phosphate electrolyte

The electrochemical behavior of FTO/CdS/PThA/PBTh was investigated in 0.2 M phosphate electrolyte (pH 6). Figure 9a shows that at ≈ 0.4 V vs Ag/AgCl, the recorded photocurrent is greater than that recorded in the dark during the cathodic scan. The manual chopping of light indicates that the assembly is highly responsive to the illumination-dark cycles. The sudden decay of photocurrent upon blocking the illumination every other second may indicate a shorter life-time of the electron before its consumption by further elementary steps of photochemical reactions. Figure 9b shows the photocurrent-time curve under a constant potential (ca − 0.500 V vs Ag/AgCl) under illumination for a longer period of time. Upon illumination of the oxygenated phosphate electrolyte (Fig. 9b), a sharp anodic current spike, similar to that which was noticed in the citrate electrolyte, is observed. Such behavior can be explained by fast charge recombination because of hole accumulations at the outermost layers of the assembly electrolyte interface. Under darkness, there is no evidence for reversed transient current. This means that no backflow of electrons from the substrate FTO to the assembly body took place.

Upon illumination of the oxygenated phosphate electrolyte (Fig. 9b (a)), a sudden increase in the photocurrent was recorded (≈ 60 μA) followed by a steady decrease in photocurrent to about 40 μA. The initial decay reflects some e/h recombination. In contrast, when the electrolyte was deoxygenated using nitrogen gas (Fig. 9b (b)), less photocurrent was recorded with behavior similar to that observed in the oxygenated solution. In the presence of a magnetic field (Fig. 9b-inset box) a small change in the recorded photocurrent in absence of O_2 was seen. Figure 9c shows the photocurrent vs time curve for the host polymer PBTh. It clearly shows lower photocurrent than that observed in Fig. 9b. This indicates that occlusion of CdS enhanced the photocurrent generation as a result of improvement of the photoinduced charge separation.

The photocurrent generated in the phosphate electrolyte is greater than that in the tested carboxylic acid electrolytes. We further investigated the effect of changing the pH on the E_{fb} of this assembly. We found no changes in E_{fb} were observed within the pH 5–8 range. We believe that a change of approximate 2 pH units did not affect the position of E_{fb} in sulfur-based assembly. The relation between E_{fb} and pH in oxide-based semiconductors is given by the following equation [39], which represents 25 mV per change in 1 pH unit:

$$E_{fb} = \text{constant} - (kT/e)\ \text{pH} \quad (2)$$

The observed change in photocurrent is due to the nature of the anion of the electrolyte, not to other factors such as change in the surface states or the coexisting OH^- anion. The fact that

Table 1 Photoelectrochemical data for the CdS/PThA/PBTh

Property	PBTh CdS/PThA/PThA	PThA	CdS
Ionization potential (IP), EV	5.4 5.6	5.28	
Band gap, E_g, eV	2.55 2.60	2.40	2.40
Electron affinity (EA)	2.85 3.0	≈ 2.90	4.45
E_{fb}, V vs SHE	0.50 ≈ 0.5	0.20	Doping-dependent

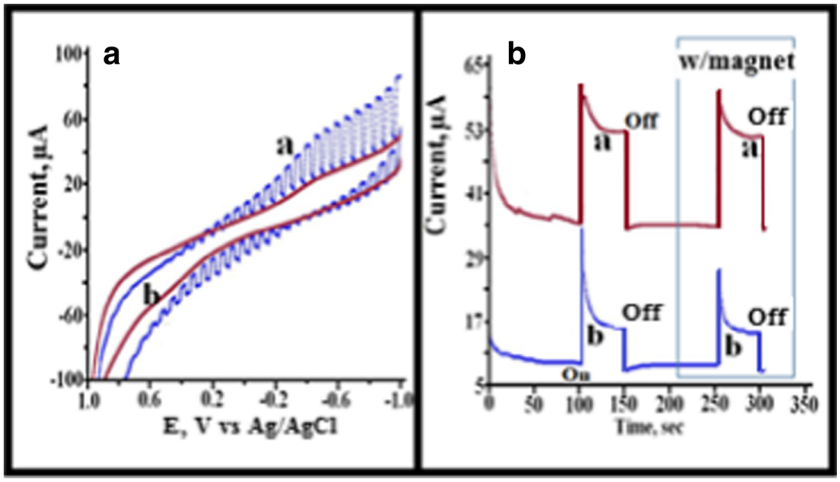

Fig. 8 Photoelectrochemical behavior of FTO/CdS/PThA/PBTh in 0.2 M Citrate electrolyte (pH 8) **a** CV at 0.1 V/s (a) illumination, (b) dark. **b** Photocurrent vs time curve at − 0.5 V vs Ag/AgCl (a) with O_2 and (b) after purge with N_2 in frame curves were collected in the presence of a magnetic field

the electrolyte anion concentration is > 0.1 M, much greater than the OH^- concentration (10^{-6} M) at pH 8, so the anion of greater concentration would be predominantly adsorbed on the electrode surface.

The role of oxygen in the photochemical activities of the assembly is highlighted in the electron consummation processes illustrated by the equation:

$$O_2 + 2e + 2H^+ \rightarrow H_2O_2 \quad (3)$$

The conjugated organic semiconductor PBTh acts as p-type semiconductor where holes are the charge carrier. When suitable photon energy hits the outermost layers of the assembly, the photogenerated holes will have a shorter diffusion course that reaches the adsorbed anions on the surface of the assembly. This suggests that the hole consummation by the used electrolyte anions is an important step in the mechanism of charge separation.

The following explains the oxidation of the studied anions at the electrolyte CdS/PThA/PBTh/electrolyte interface.

In phosphate electrolyte, formation of phosphate radical anion is one way to prevent the e/h recombination process according to Eq. 3:

$$HPO_4^{-2}{}_{(aq)} + h\ldots \rightarrow HPO_4^{-}{}_{(aq)} \quad (4)$$

The formation of HPO_4^- has been reported by others [40]. Equations 2 and 3 explain how oxygen and phosphate participate in the charge separation process that lowers the e/h recombination.

In the presence of acetate or citrate electrolyte, the photo-oxidations of acetate or citrate anions achieve a Kolb-type reaction [41]. In the presence of simple R (COO^-) ions such as acetate, the following reaction takes place [41] as illustrated in Eq. 4:

$$R\ (COO^-)_{(aq)}\ldots + h \rightarrow R._{(aq)}\ldots + CO_{2\ (gas)} \quad (5)$$

The large concentration of the studied anions (0.2 M) allowed these anions to dominate the hole consumption

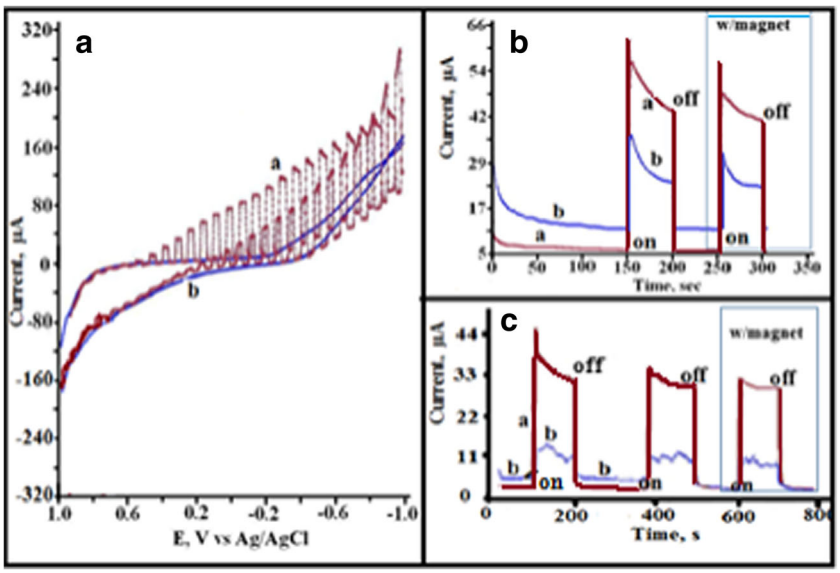

Fig. 9 Photoelectrochemical behavior of FTO/CdS/PThA/PBTh in 0.2 M phosphate electrolyte (pH 6). **a** CV at 0.1 V/s (a) illumination and (b) dark. **b** Photocurrent vs time curve at − 0.5 V vs Ag/AgCl (a) with O_2 and (b) after purge with N_2 and **c** photocurrent vs time curve of FTO/PBTh only at − 0.5 V vs Ag/AgCl (a) with O_2 and (b) after purge with N_2 in box curve indicate the presence of a magnetic field

Table 2 Charge transport data for the CdS/PThA/PBTh (5.094 μm)

Electrolyte	Electron-life time[a] (τ_n), s	Electron-diffusion coefficient, $cm^2\ s^{-1}$	Estimate electron-transport time (τ_r), s
Phosphate	0.106	2.96×10^{-6}	0.045
Acetate	0.100	3.14×10^{-6}	0.042
Citrate	0.316	9.9×10^{-7}	0.135

[a] Calculated using Eq. 1

process as illustrated in Eqs. 3, 4, and 5. This increased the charge separation as indicated by the recorded large photocurrent at more negative potential than − 0.5 V vs Ag/AgCl.

3.2.4 Electron lifetime (τ_n) in FTO/CdS/PThA/PBTh

The changes in the open circuit potentials (dV_{opn}) of photoelectrochemical cells in acetate, citrate, and phosphate electrolytes were used in Eq. 1. An estimation of electron lifetime at this interface in each electrolyte was obtained. The results are listed in Table 1.

The data listed in Table 1 indicate that τ_n is the shortest in the phosphate and acetate electrolytes and longest in the citrate electrolyte. The comparison of the magnitude of the photocurrents during the illumination period in the photocurrent vs time plots (Figs. 7, 8, and 9b) shows that the phosphate electrolyte produced the largest photocurrent (≈ 41 μA). The electron lifetime (τ_n) represents the electron recombination time constant. This relates to an electron diffusion length L according to the following formula [42]:

$$L = (D_e\ \tau_n)^{\S} \tag{6}$$

where D_e is the electron diffusion coefficient. Efficient collection of photogenerated electrons requires that L should be greater than the film thickness. The results listed in Table 2 suggest that D_e is $\approx 3.0 \times 10^{-6}$ cm^2/s in acetate, is $\approx 2.96 \times 10^{-6}$ cm^2/s in phosphate, and is $\approx 9.9 \times 10^{-7}$ cm^2/s in citrate. The assembly films do not possess even thickness but rather irregular surfaces with minimum and maximum thicknesses (Fig. 10). This suggests that most of the photoactivities took place within the film minima as the electron diffusion length is longer than film thickness at these locations. The host polymer, PBTh in phosphate electrolyte, the τ_n was 500 ms. Equation 5 shows that D_e within the host polymer PBTh only in phosphate electrolyte is $\approx 6.27 \times 10^{-7}$ cm^2/s. This value leads to an estimate of τ_r (electron transport time) of 200 ms. Comparing this with the data listed in Table 2 clearly indicates that occlusion of CdS decreased τ_r and increased both D_e and L, which enhances the generation of photocurrent.

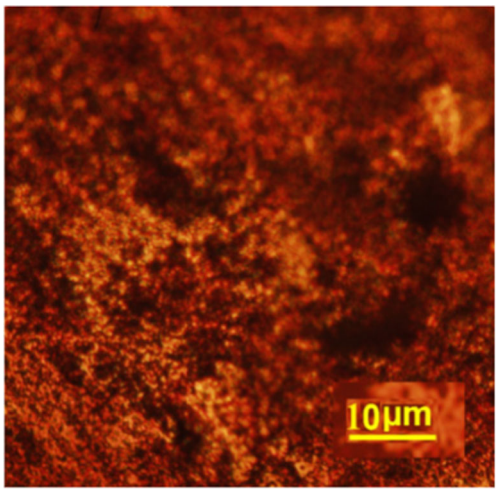

Fig. 10 microscopic image of 6 μm of the CdS/PThA/PBTh Film on FTO

3.2.5 Magnetic field effect on the OOI

The experimental setup for the magnetic study is displayed in Fig. 1. The photocurrent of FTO/CdS/PThA/PBTh in the absence and presence of a magnetic field is displayed in Figs. 7, 8, and 9 (inset boxes). Little change of photocurrent can be noticed when a 0.2-T magnetic field is applied. These result suggest that the electrolyte's anions are an important factor in CdS/PThA/PBTh assembly's response to the magnetic field. For example, during the illumination period, the photocurrent decreased in all studied electrolytes except acetate. Upon illumination, unpaired electrons are generated. This creates organic paramagnetism with a random spin. The response of organic paramagnetism to the magnet depends on several factors, such as the spin of electron/hole pairs, existence of singlet and triplet states, interaction of donor anions (HPO_4^{-2}, $C_3H_5O(COO)_3^{3-}$, and CH_3COO^-) with the excitons generated at this interface, and the intersystem crossing. The fact that the magnetic field has no effect on the illuminated thin film of CdS suggests that both the PBTh and PThA components of this assembly were responsible for the behavior recorded in these figures. The presence of oxygen in the electrolytes helps in charge separation by the formation of O_2^-. During its life time, this anion radical acted as a temporary molecular paramagnet [36] that interfered with the applied magnetic field and generated the inconsistent photocurrent outcome shown in Figs. 6, 7, 8, and 9b. Previously detailed studies on magnetic field effects on the dye-sensitized solar cells [43] concluded that the presence of a magnetic field causes slowing of the spin

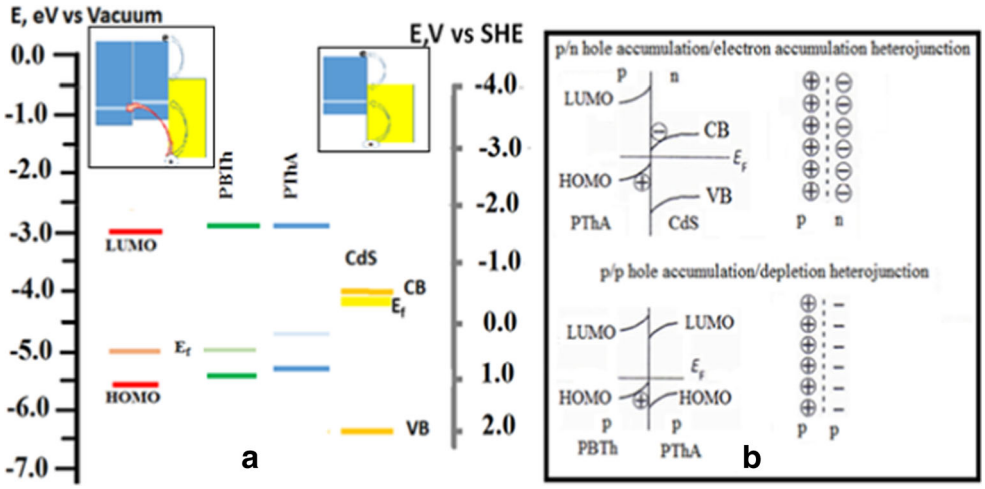

Fig. 11 **a** Energy map for CdS/PThA/PBTh interface. **b** Heterojunction hole/electron activities.[⊖] electron accumulation, [⊕] hole accumulation, [−] hole depletion)

of interfacial electron/hole pairs at a frequency dependent on a field strength. Previous studies [44] suggested that a low-intensity magnetic field can induce enhancement of electrolyte ion movement and reduce charge transfer resistance resulting in an increase of both capacitance and energy density.

3.3 Band-energy map of CdS/PThA/PBTh

The data obtained from optical and electrochemical measurements in Figs. 2, 7, 8, and 9 were used to calculate the ionization potential (IP) and electron affinity (EA) and Fermi level (E_{fb}) of CdS/PThA/PBTh. These important parameters, along with the approximate value of the band gap (E_g), were used to draw an energy map of CdS/PThA/PBTh. These parameters are also needed to explain the electrical and optical properties of the film. The IP, EA, and E_{fb} were calculated using formulas derived elsewhere [10].

These results are discussed in terms of how possible band alignment between the p-type organic polymers with its diffusional HOMO/LUMO border and the amorphous n-type CdS nanoparticles may affect the generation of unpaired electrons upon illumination of the interface. The PBTh, PThA, and amorphous CdS have band gaps that allow absorption of wavelengths in the visible spectrum which makes both materials and their I/O/O/I assemblies potentially useful as photoelectrochemical device components.

A list of photoelectrochemical data for PBTh, PThA, CdS, and CdS/PThA/PBTh is summarized in Table 1 and Fig. 11a. Figure 11a insets illustrates the formation of a hybrid sub-band energy level that facilitates charge transfer at the CdS/PThA/PBTh. At the I/O/O/I, a strong hybridization between electron-like and hole-like sub-band states occurs in close proximity to the Fermi energy level. The hole barrier height calculated from the difference between the energy level of the hybrid band and valance band (VB) of CdS is ~ 1.5 eV. This is ~ 1.5 V more negative than the CdS VB. With the hybrid band at this more negative potential attraction, the hole is stronger and makes the charge transfer process possible. In contrast, the electron barrier height is ~ 0.9 eV which is ~ 0.9 V more positive than the potential of the electrons in the LUMO of PThA. However, if we consider that electrons in the organic part of the IOOI are concentrated at a lower energy level than the LUMO, due to indirect band gaps existing in the assembly, then, the electron barrier height will be even lower than the calculated value (~ 0.9 eV). This would also make hole transfer more thermodynamically favorable than electron transfer, as 1.5 V is more attractive for holes than 0.9 V is to electrons. We realize that our conclusions are just a general outline of the possible energy map in the created assembly. The photoactivity outcome from the assemblies CdS/PThA/PBTh can be simplified by Fig. 11b. The outcome character of the assemblies was of a p-type. The charge transfer process involved reduction of O_2 to H_2O_2 and oxidation of the electrolyte anions. Figure 11b suggests charge activities between CdS/PThA and charge activities between PBTh/PThA interfaces. The details of the charge transfer mechanism may follow a Dexter-type [45] mechanism that can be viewed as a pair of simultaneous hole and electron-transfer events.

4 Conclusion

Table 1 indicates that the presence of CdS in organic films of polybithiophene did not cause large changes in the energy band structure compared with that of the host thiophene polymer. The photoelectrochemical outcome was dominated by the polybithiophene. The optical properties of the created assemblies indicates that occlusion of modified CdS nanoparticles into the network structure of PBTh inhibits the energy dissipation process and decreases the optical conductivity of the host polymer. Photoelectrochemical results show that the behavioral outcome of the assemblies reflects formation of hybrid sub-bands as a product of band alignments between the organic film and CdS. Furthermore, inclusion of CdS in

the thiophene-based polymers played an important role in the charge separation and transfer processes by enhancing the charge separation and consequently increasing the resulted photocurrent. The magnetic field affected the photogeneration of singlet/triplet radical pairing process.

Acknowledgements The authors acknowledge the Office of Academic Affairs at the Indiana University Kokomo for supporting this project.

Compliance with ethical standards

Conflict of interest The authors declare that they have no conflict of interest.

References

1. Su C, Yang F, Ye Y, Xu L, Wang L, Zhang C (2013) Poly[tris(thienylphenyl) amine] derivatives as a performance-improved cathode material for lithium ion batteries. J Electrochem Soc 160(11):A2021–A2026
2. Zhang M, Wu Z, Wang Q, Song Q, Ding Y (2010) Synthesis and properties of a new [60] fullerene-donor system containing dicyanovinyl groups. Mater Lett 64(20):2244–2246
3. Shirota Y (2005) Photo- and electroactive amorphous molecular materials—molecular design, syntheses, reactions, properties, and applications. J Mater Chem 15:75–93
4. Tada A, Geng Y, Wei Q, Hashimoto K, Tajima K (2011) Tailoring organic heterojunction interfaces in bilayer polymer photovoltaic devices. Nat Mater 10:450–455. https://doi.org/10.1038/nmat3026
5. Walzer K, Maennig B, Pfeiffer M, Leo K (2007) Highly efficient organic devices based on electrically doped transport layers. Chem Rev 107:1233–1271
6. Shirota YJ (2000) Organic materials for electronic and optoelectronic devices. J Mater Chem (10): 101–25
7. Zeng HP, Wang TT, Sandanayaka SD, Araki Y, Ito O (2005) Photoinduced charge separation and charge recombination in [60]fullerene−ethylcarbazole and [60]fullerene−triphenylamines in polar solvents. J Phys Chem A 109(21):4713–4720
8. Kageyama H, Shirota Y (2007) Charge carrier transporting molecular materials and their applications in devices. Chem Rev 107(4): 953–1010
9. Wei H, Yan X, Wu S, Luo Z, Wei S, Guo Z (2012) Electropolymerized polyaniline stabilized tungsten oxide nanocomposite films: electrochromic behavior and electrochemical energy storage. J Phys Chem C 116:25052–25064
10. Slawomir Braun X, Osikowicz W, Wang Y, Salaneck WR (2007) Energy level alignment regimes at hybrid organic–organic and inorganic–organic interfaces. Org Electron 8(1):14–20
11. Osikowicz W, de Jong MP, Salaneck WR (2007) Alignment of C60 and poly 3TH. Adv Mater 19:4213
12. Wan A, Hwang J, Amy F, Kahn A (2005) Impact of electrode contamination on the αNPD/Au hole injection barrier. Org Electron 6:47
13. Slawomir B, William Salaneck R, Fahlman M (2001) Energy-level alignment at organic/metal and organic/organic interfaces. Adv Mater 21:1450–1472
14. Klenkler RA, Xu G, Zoran DP (2007) Charge injection at interfaces between molecularly doped polymer thin films. Appl Phys Lett 90: 092106. https://doi.org/10.1063/1.2709936
15. de Freitas JN, Grova IR, Akcelrud LC, Arici E, Serdar Sariciftcic N, Nogueir AF (2010) The effects of CdSe incorporation into bulk heterojunction solar cells. J Mat Chem 20:4845
16. Ananthakumar S, Ramkumar J, Moorthy Babu S (2014) Synthesis of thiol modified CdSe nanoparticles/P3HT blends for hybrid solar cell structures. Mater Sci Semicond Process 22:44–49
17. Otero M, Dittrich T, Rappich J, Heredia DA, Fungo F, Durantini E, Otero L (2015) Photoinduced charge separation in organic-inorganic hybrid system: C60-containing electropolymer/CdSe-quantum dots. Electrochim Acta 173(10):316–322
18. Grynko DO, Fedoryak OM, Smertenko PS, Ogurtsov NA, Pud AA, Noskov, Yu V, Dimitriev OP (2015) Multifunctional role of nanostructured CdS interfacial layers in hybrid solar cells. Nanosci Nanotechnol 15(1):752–758
19. Liu T, Mai X, Chen H, Ren J, Liu Z, Li Y, Gao L, Wang N, Zhang J, He H, Guo Z (2018) Carbon nanotube aerogel–CoS_2 hybrid catalytic counter electrodes for enhanced photovoltaic performance dye-sensitized solar cells. Nanoscale 10:4194–4201. https://doi.org/10.1039/C7NR09260A
20. Wei H, Yan X, Li Y, Wu S, Wang A, Wei S, Guo Z (2012) Hybrid electrochromic fluorescent poly (DNTD)/CdSe@ZnS composite films. J Phys Chem C 116(7):4500–4510. https://doi.org/10.1021/jp2117906
21. Chen Y, Tamblyn I, Quek SY (2017) Energy level alignment at hybridized organic–metal interfaces: the role of many-electron effects. J Phys Chem C 121(24):13125–13134
22. Zhong Y, Tada A, Geng Y, Wei Q, Hashimoto K, Tajima K (2013) Donor/acceptor interface modifications in organic solar cells. J Photopolym Sci Technol 26(2):181–184
23. Keddam M, Senyarich S, Takenouti H, Bernard P (1994) A composite electrode for studying powdered electroactive materials: preparation and performance. J Appl Electrochem 24:1037
24. Anani A, Mao Z, Srinivasan S, Appleby AJ (1991) Dispersion deposition of metal—particle composites and the evaluation of dispersion deposited nickel—lanthanum nickelate electrocatalyst for hydrogen evolution. J Appl Electrochem 21(8):683–689
25. HOVESTAD A, JANSSEN LJJ (1995) Electrochemical codeposition of inert particles in a metallic matrix. J apply Electrochem 25:519–527
26. de Tacconi NR, Wenren H, Rajeshwar K (1997) Photoelectrochemical behavior of nanocomposite films of cadmium sulfide, or titanium dioxide, and nickel. J of Electrochem Soc 144(9):3159–3163
27. Kasem K, Olsen JC, Baker K, Santucci C, Lalla J, Willman AN (2016) Electrochemical studies on a photoactive. Synth Met 217: 61–67
28. Zhou M, Lin W-Y, de Tacconi NR, Rajeshwar K (1996) Metal/semiconductor electrocomposite photoelectrodes. J Electroanal Chem 402:221–224
29. Beck P, Dahhaus M, N. Zahedi N. (1992) Anodic codeposition of polypyrrole and dispersed TiO_2. Electrochem Acta 37:1265
30. De La Cruze TEC, Ambrosio Lazaro RC, Mota Gonzalez ML, Luque PA, Castillo SJ, Carrillo- Castillo A. (2015) A simple method for the synthesis of CdS nanoparticles using a novel surfactant. Chalcogenide Lett 12(4):147–153
31. Zaban A, Greenstien M, Bisquert J (2003) Determination of the electron life time in monocrystalline dye solar cells by open–circuit voltage decay measurements. Chem Physics Chem 4:859
32. Tauc J (1968) Optical properties and electronic structure of amorphous Ge and Si. Mater Res Bull 3:37–46
33. Dressel M (2002) Electrodynamics of solids optical properties of electrons in matter, editor George Grüner. Cambridge university press, Cambridge
34. Pankaj S, Katyal SC (2007) Determination of optical parameters of alfa $(As_2Se_3)_{90}Ge_{10}$ thin film. J Phys D Appl Phys 40(7):2115–2120

35. Wu MT, Yao X, Yuan ZH, Sun HT, Wu WC, Chen OH, Xu GY (1993) Effect of noble metal catalyst on titania exhaust gas oxygen sensor. Sensors Actuators B 14:491
36. Seraghni N, Belattar S, Mameri Y, Debbache N, Sehili T (2012) Fe (III)-citrate-complex-induced photooxidation of 3-methylphenol in aqueous solution. Int J Photoenergy 2012:630425, 10 pages. https://doi.org/10.1155/2012/630425
37. Kasem KK, Elmasry M, Baker K, Santucci C (2017) Photoelectrochemical and magnetic studies on photoactive interface thin solid film assemblies. Thin Solid Films 634:56–65
38. Sookhakian M, Amin YM, Baradaran S, Tajabadi MT, MoradiGolsheikh A, and Basirun WJ (2014) A layer-by-layer assembled graphene/zinc sulfide/polypyrrole thin-film electrode via electrophoretic deposition for solar cells. Thin Solid Films, 204–211
39. Gerischer H (1970) In Physical Chemistry. An advanced treatise, H. Eyring, ed. Academic Press, New York. 9:463–542
40. Abdullah M, Low GKC, Matthews RW (1990) Effects of common inorganic anions on rates of photocatalytic oxidation of organic carbon over illuminated titanium dioxide. J Phys Chem 94(17): 6820–6825
41. Cerviño RM, Triaca WE, Arvía AJ (1984) Phenomenology related to the kinetics of Kolbe electrosynthesis. J Electroanal Chem 172: 255–264
42. Zhao Y, Nardes AM, Zhu K (2014) Solid state mesostructured peroveskite CH3NH2PbI3 solar cells. J Physical Chemistry Lett 5(5):490–494
43. Klein M, Pankiewicz R, Zalas M, Stampor W (2016) Magnetic field effects on dye sensitized solar cells controlled by different cell architecture. Sci Rep 6:30077
44. Wei H, Gu H, Guo J, Cui D, Yan X, Liu J, Cao D, Wang X, Wei S, Guo Z (2017) Significantly enhanced energy density of magnetite/polypyrrole nanocomposite capacitors at high rates by low magnetic fields. Adv Compos Hybrid Mater 1(1):127–134. https://doi.org/10.1007/s42114-017-0003-4
45. Dance ZEX, Ahrens MJ, Vega AM, Ricks AB, McCamant DW, Ratner MA, Wasielewski MR (2008) Direct observation of the preference of hole transfer over electron transfer for radical ion pair recombination in donor-bridge-acceptor molecules. J Am Chem Soc 130:830–832